Dynamic Phase Synchrony based Ranked Spatio-Temporal Clustering for Tracking Time-Resolved Functional Brain Networks

Priya Aggarwal[a,*], Anubha Gupta[a]

[a]*SBILab, Department of Electronics and Communication Engineering, Indraprastha Institute of Information Technology-Delhi (IIIT-D), Delhi, India*

Abstract

Of late, there has been a growing interest in studying brain networks, particularly, for understanding spontaneous temporal changes in functional brain networks. Recently, phase synchrony based methods have been proposed to track instantaneous time resolved functional connectivity without any need of windowing the data. This paper extends one such recently used phase synchrony measure in two steps. First, multiple temporal models are built from three-mode spatio-temporal tensors that are further clustered to detect overlapping dynamic brain network communities. This clustering is based on spatio-temporal data and hence, is named as *Spatio-Temporal Clustering* (STC). Second, a method is proposed to rank all the communities allowing the proposed model to deal with multiple communities of differing time evolution. This helps in the comparison of network communities, especially, when available communities are too dense to provide relevant information for comparison. The ranking of communities allows for the dimensionality reduction of communities, while still maintaining the key brain networks. Intrinsic time varying functional connectivity has been investigated for large scale brain networks, including default-mode network (DMN), visual network (VN), cognitive control network (CCN), auditory network (AN), etc. The proposed method provides a new complementary tool to investigate dynamic network states at a high temporal resolution and is tested on resting-state functional MRI data of 26 typically developing controls (TDC) and 35 autism spectrum disorder (ASD) subjects. Simulation results demonstrate that ASD subjects have altered dynamic brain networks relative to those of TDC.

Keywords: Functional MRI, Resting-state brain networks, Dynamic functional connectivity, Instantaneous phase synchrony, Autism spectrum disorder, Nonlinear time series analysis

1. Introduction

Functional connectivity analysis in brain is an important method in neuroscience for functional brain networks discovery [1, 2, 3]. The functional Magnetic Resonance Imaging (fMRI) provides information about large-scale functional brain networks such as visual network (VN), somato-motor Network (SMN), auditory network (AN), cognitive control network (CCN), default-mode network (DMN) etc. [4, 5, 6, 7, 8]. The conventional static connectivity analysis only captures brain networks that are present over the entire duration of scan and therefore, fails to account for the time varying nature of brain networks. Owing to this, dynamic functional connectivity (dFC) is a cardinal way to capture and characterize dynamic brain networks [9, 10, 11] supported by a growing body of research suggesting for dynamic reconfiguration of brain networks [12, 13, 14, 15, 16, 17].

A sliding-window (SW) approach is commonly used on fMRI time series data to elucidate dynamic aspects of functional brain networks (see [18] for review). In this approach, brain networks are assumed to be time-invariant within a predefined window duration. This window is subsequently shifted either by one or many time points, thereby, estimating temporal changes in brain networks. However, this method is suboptimal due to the strong dependence of the window size and the overlap between

*Corresponding author

Email addresses: priyaa@iiitd.ac.in (Priya Aggarwal), anubha@iiitd.ac.in (Anubha Gupta)

windows to explore fluctuations in dFC [19, 20]. Moreover, there may be abrupt changes in the functional connectivity at different time points. Hence, fixed window assumption of SW analysis may not necessarily hold true [21].

Besides considering conventional SW approach, other attempts have been made to find instantaneous patterns of dFC without windowing and hence, with no need of struggling with choosing the right window length [22, 23, 24, 25, 26]. Phase difference between the time series of regions is one such instantaneous measure of dFC and is commonly known as phase synchrony. This approach computes connectivity at every time point and hence, alleviates the need of choosing window length. Moreover, this method allows extraction of dynamic functional connectivity at higher temporal resolution compared to the state-of-the-art sliding-window approach. To date, very few studies have utilized phase synchrony measure to compute dFC in resting state fMRI [22, 23, 24, 25, 26].

In the present study, we seek whole-brain dynamic brain networks' topology using instantaneous phase measure. Instantaneous phase from signals can be computed using the Hilbert transform [22], wherein a signal is first bandpass filtered. Next, instantaneous phase is estimated from the signal's analytic form obtained from the Hilbert transform. We propose to use this measure to build dynamic brain networks.

After obtaining dFC, next task is to identify communities of densely connected regions and to study their temporally dynamic profiles from multiple temporal snapshots of phase synchrony matrices. Related work of identifying communities using phase-synchrony based time-varying matrices is implemented by decomposing a three-mode tensor of regional connectivity at different times and then analyzing and linking the changes in the community structures [23]. For example, tensor decomposition based method on three-mode tensor (region $\times$ region $\times$ time) is applied to obtain a few significant components [23]. Each component consists of three vectors, namely, loading vectors. First two loading vectors are related to regions and are used to generate communities. The third loading vector contains temporal information for tracking a community's time-varying dynamic profile. However, we observe that direct utilization of tensor decomposition fails to provide a good model for dynamic brain network communities due to random fluctuation of loading vectors related to regions. It renders unclear interpretations of these vectors.

To overcome the above issue, we propose a Spatio-Temporal Clustering (STC) framework based on the temporal models learned from tensor decomposed loading vectors. Our framework identifies multiple clusters from each temporal model. This results in many clusters, with a time loading vector for each cluster. With a "hub" of identified clusters, we rank them using our proposed Combined Cluster Score (CCS) based on edge values between regions in a cluster and corresponding temporal loading vector. Thus, we obtain significant dynamic brain network (DBN) communities. We will formalize our proposed model in the next few sections.

The major contributions of this work are as follows:

- We provide a spatio-temporal clustering framework to detect dynamic brain network communities using K-means clustering and Silhouette criterion. Our model allows a region to belong to multiple network communities and hence, provides a novel method to detect overlapping dynamic brain network communities at the highest possible temporal resolution of acquired data.
- We provide a method to rank all the clusters that allows our model to deal with a large hub of multiple clusters having different temporal evolution. This helps with the comparison of network communities, especially when available communities are too dense to provide relevant information for comparison.
- We differentiate subjects suffering with autism spectrum disorder from healthy controls using the proposed dynamic functional connectivity analysis. In addition, we provide new analysis tool to explore dynamic functional connectivity and characterize relationship between region of interests (ROIs) without explicitly defining window length as required in the conventional 'sliding window' based dynamic functional connectivity analysis.

The organization of this paper is as follows: Section 2 describes materials used in this paper. Section 3 explains the steps to learn and track dynamic brain network communities and their temporal evolution profile. Section 4 reports experiments with real data. In the end, discussion and conclusions are presented in section 5 and 6, respectively.

Notations: We use lowercase boldface letters for vectors (e.g. $\boldsymbol{a}$), capital boldface letters for matrices (e.g. $\mathbf{A}$), italics letters for scalars (e.g. a or A), and Euler script letters for tensors (e.g. $\mathcal{A}$).

2. Materials

2.0.1. Data Acquisition

In this paper, we have used publicly available Autism dataset contributed by Georgetown University, a collection site of Autism Brain Image Data Exchange II (ABIDEII) `http://fcon_1000.projects.nitrc.org/indi/abide/`. This dataset is comprised of fMRI data of 55 healthy subjects (Typically Developing Controls (TDC)) (8.1−13.8 years) and 51 Autism Spectrum Disorder (ASD) subjects (8.1−13.9 years). This data has been collected with Echo Time (TE) equal to 30 ms and Repetition Time (TR) equal to 2000 ms. The fMRI brain data is collected over 152 brain volumes. Each brain volume consists of acquisition of 43 brain slices with dimension 64×64. A three-dimensional structural magnetization prepared rapid gradient echo $T1$-weighted image is acquired for every subject with TR = 2530 ms, flip angle = 7°, FOV = 256×256 mm^2, and the number of brain slices equal to 176.

2.0.2. Data Preprocessing

fMRI data are pre-processed using SPM12 (Statistical Parametric Mapping; `http://www.fil.ion.ucl.ac.uk/spm/software/spm12/`). Preprocessing of resting state fMRI dataset starts with the removal of first few volumes to allow the magnetization to reach to the steady state value. We discarded first five volumes. The other functional volumes are slice time corrected using the middle slice as a reference followed by motion correction. Functional scans are spatially normalized onto the Montreal Neurological Institute (MNI) space using DARTEL procedure, i.e., using transformation parameters provided by the $T1$-weighted image normalization, resulting in functional images of dimension $53 \times 63 \times 52$ (resampled to 3-mm isotropic voxels). Further, data is smoothed with a Gaussian kernel with 6 mm full width half maximum.

Finally, we regress out nuisance variables (6 head motion parameters, average cerebro-spinal fluid signal from ventricular masks, and average white matter signal from white matter mask) from each voxel's time series followed by bandpass filtering using a butterworth filter to reduce the low frequency drift and high frequency noise. Hilbert transform is computed for narrowband filtered signals and hence, requires prefiltering of signals. To this end, we bandpass filtered the data in the frequency range of 0.01 to 0.08 Hz. In general, this bandwidth filtering in fMRI is believed to minimize the low frequency drift and the high frequency noise.

Temporal artifacts were identified in each subject's data by calculating the framewise displacement (FD) from the derivatives of the six rigid-body realignment parameters estimated during motion correction preprocessing step [27]. Subjects with more than 45 brain volumes (30% of total brain volumes) having FD > 0.5 mm were excluded from further analysis (TDC group 4/55; ASD group 12/51). We did not perform scrubbing of data because this may lead to alterations in the temporal structure of images [27].

We have only included male subjects in the study because brain network differences associated with gender may confound differences across the TDC versus ASD groups. After quality control, a total of 26 TDC and 35 ASD subjects remained for our analysis. A two-sample t-test with unequal variance showed no significant difference (at $p < 0.05$ significance level) in the age of two groups as shown in Table-1.

2.0.3. Brain Parcellation

Following preprocessing, whole brain data is parcellated into 90 anatomical predefined ROIs via Automated Anatomical Labeling (AAL) atlas [28]. In this atlas, 45 ROIs lie in the left brain hemisphere and 45 ROIs lie in the right brain hemisphere. Table-S1 lists these 45 ROIs, where odd numbers represent left hemisphere ROIs and even numbers represent right hemisphere ROIs. In order to find region-representative time series for every ROI, we averaged time-series of all voxels belonging to the same ROI. This resulted into a matrix $\mathbf{X}$ of dimension $T \times N$, where T denotes the number of time points (or the number of times a brain volume is scanned) such as 147 for a given subject's fMRI data and N denotes the number of ROIs such as 90 for the AAL atlas.

3. Learning and Tracking Dynamic Brain Network Communities

This section describes proposed steps for identifying underlying dynamic brain networks. Fig.1

Table 1: Summary of TDC versus ASD Subjects' Data

Characteristic	TDC (S=26)	ASD (S=35)	p-value
Gender	Male	Male	
Age (years)			
Mean (SD)	10.9 (1.62)	11.17 (1.49)	0.50
Range	8.06−13.79	8.25−13.91	
Full Scale IQ			
Mean (SD)	120.32 (13.53)	119.06¶ (14.18)	0.73
Range	91−148	95−149	
ADI-R			
Social total A	–	19.74¶ (5.28)	
Verbal total BV	–	14.97¶ (4.91)	
RRB total C	–	5.09¶ (2.38)	
R Onset total D	–	2.56¶ (1.23)	
ADOS			
Total	–	10.52ϒ (4.61)	
Communication	–	3.18ϒ(1.54)	
Social	–	7.33ϒ (3.53)	
Stereo Behavior	–	1.89ϒ (1.58)	

TDC: Typically Developing Control; ASD: Autism Spectrum Disorder; ADI-R: Autism Diagnostic Interview-Revised; Social total A: Reciprocal Social Interaction Subscore A; Verbal total BV: Abnormalities in Verbal Communication Subscore; RRB total C: Restricted, Repetitive, and Stereotyped Patterns of Behavior; ADOS: Autism Diagnostic Observation; Stereo Behavior: Stereotyped Behaviors and Restricted Interest. Column on the right displays p-values for two sample t-test for each sample characteristic. ¶One subject's score is missing. ϒSeven ASD subjects do not have these scores. '−' signifies that these scores are not available for the TDC group.

illustrates a schematic of these steps presented as below:

- In the first step, we utilize phase synchrony based instantaneous measure to compute adjacency matrices of dynamic functional connectivity. We compute these matrices at each time instant and for all subjects.
- Second step involves subject-summarization of three-mode spatio-subject tensor (region × region × subject) at each time instant that leads to (region × region) single adjacency matrix at every time point. Similar processing at all time points results in a three-mode spatio-temporal tensor (region × region × time).
- Thirdly, subject-summarized spatio-temporal tensor is decomposed via tensor decomposition into multiple components. We utilize these components to learn multiple temporal models representing brain regions evolving over time.
- Next, K-means clustering is used to extract clusters from each learned temporal model in the previous step.
- Last, we rank identified clusters using our proposed cluster scoring metric. Clusters with high scores are labeled as dynamic brain networks that are identified at group-level.

We explain elaborately each of the above steps in next few subsections.

3.1. Time Varying Phase Synchrony Measure

Once pre-processing of BOLD data is complete, we compute phase synchrony based dynamic connectivity matrices between ROIs at all time instants. This allows greater temporal resolution of dynamic functional connectivity compared to the state-of-the-art SW approach.

Hilbert transform of averaged BOLD time series of each ROI is computed to obtain analytic signals, written as $A(t)cos(\varphi(t)))$, where $A(t)$ and $\varphi(t)$ denote the instantaneous amplitude and instantaneous phase, respectively. Please note that we have removed first and last ten time points from further analysis in order to reduce border effects caused by Hilbert transform. For any two i and j ROIs, pairwise phase difference ranged between 0 to π is computed as:

$$\Delta\varphi_{ij} = \begin{cases} |\varphi_i - \varphi_j|, & if \ |\varphi_i - \varphi_j| \leq \pi \\ 2\pi - |\varphi_i - \varphi_j|, & otherwise \end{cases} \quad (1)$$

Using the pairwise phase differences of all pairs of ROIs, the instantaneous coupling matrix (ICM) $\mathbf{C}(t)$, normalized between 0 to 1, is computed as

$$C_{ij}(t) = 1 - \Delta\varphi_{ij}/\pi. \quad (2)$$

Please note that matrix $\mathbf{C}(t)$ in the above equation contains values between 0 (perfect phase matching) and 1 (no phase matching). Next, we converted this matrix into sparse, undirected binary matrix using thresholding, as has been done previously in [23, 25] for phase synchrony based fMRI

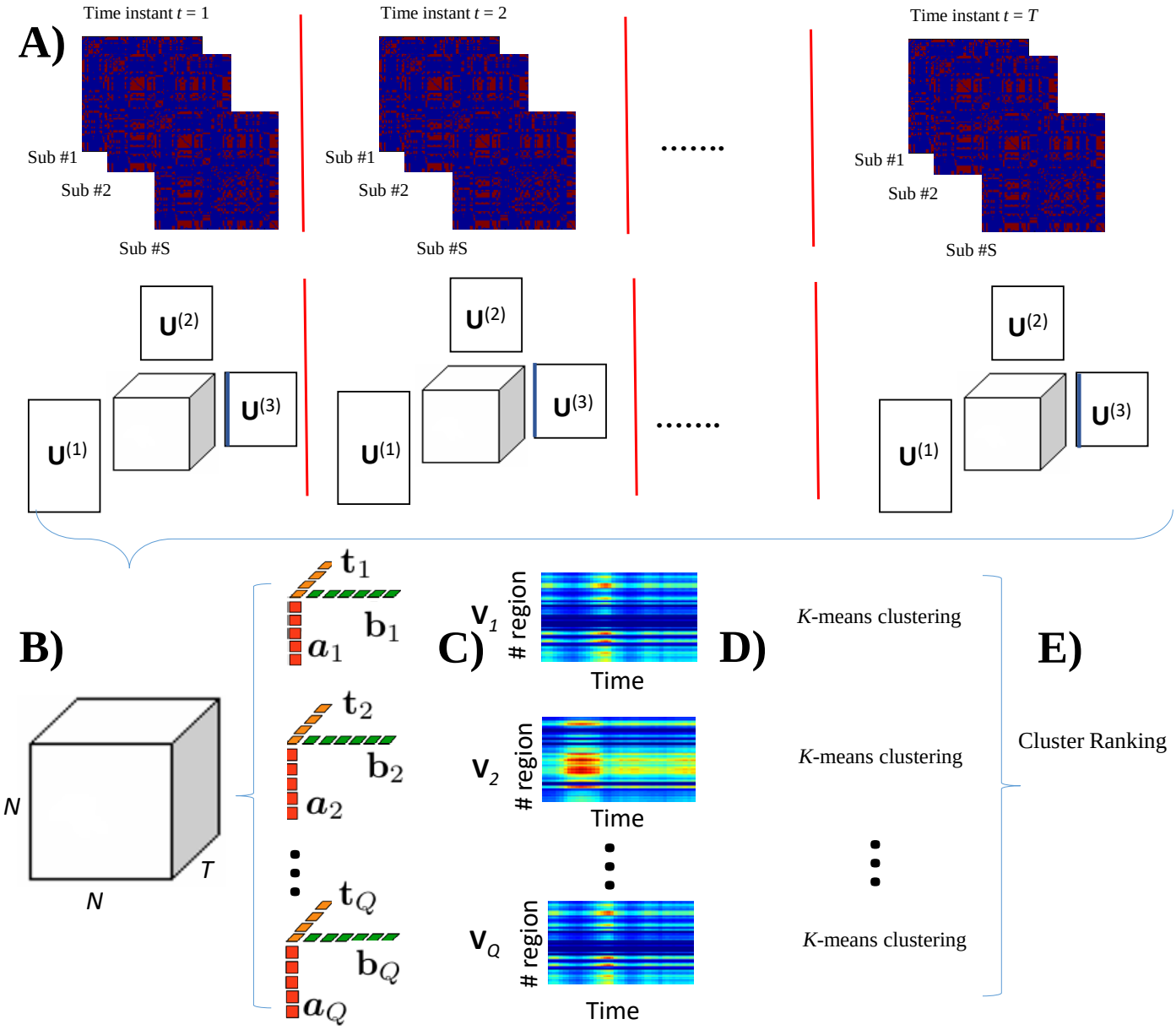

Figure 1: A) High resolution binarized instantaneous coupling matrices are summarized by subjects at each time instant, B) Resulting three-mode tensor of dimension $N \times N \times T$ is decomposed using PARAFAC decomposition with Q factors where the first and second components represent region loading vectors and the third component represents the time loading vector. C) The temporal model of ROIs in each component is represented by matrix $\mathbf{V}_q$ $(q = 1, 2, ..., Q)$. D) K-means clustering is used to obtain dynamic brain network (DBN) communities from each temporal model. E) DBN communities are ranked using our combined cluster score (CCS) presented in section 3.5 to obtain significant dynamic brain networks.

experiments. Hence, binarized instantaneous coupling matrix $\mathbf{C}^b(t)$ from $\mathbf{C}(t)$ is computed as:

$$C^b_{ij}(t) = \begin{cases} C_{ij}(t) = 1, & \Delta\varphi_{ij} < \tau \\ C_{ij}(t) = 0, & otherwise \end{cases} \quad (3)$$

where τ denotes threshold on pairwise phase differences matrix $\Delta\varphi_{ij}$ that is ranged from 0 to π. Recently in [23], $\frac{\pi}{6}$ value is used to threshold ICM, i.e., positions with pairwise phase difference of more than $\frac{\pi}{6}$ are set to zero in ICM . We have utilized the same value of τ in (3) to obtain $\mathbf{C}^b(t)$. We denote this matrix as binarized instantaneous coupling matrix (BICM).

To validate our choice of threshold, we also considered an edge threshold of 30% (i.e., retaining the bottom 30% connections of ICM at each time instant) that are being considered as biologically significant edges in many previous studies [29, 30, 31]. However, the bottom 30% edge threshold results in high thresholding value upto $\frac{\pi}{3}$ at some time instants. Moreover, it is not necessarily true that a fixed number of edges will be active all the times. Hence, in order to avoid any bias from results due to the choice of threshold, all experiments are performed with a fixed threshold of $\frac{\pi}{6}$ as has been done in [23] instead of choosing some fixed number of significant edges.

Thus, $\mathbf{C}^b_s(t)$ is the adjacency matrix at time t for any subject s. The collection of $\mathbf{C}^b_s(t)$ for all subjects $s = 1, 2, ..., S$, in each TDC and ASD group, form three-mode spatio-subject tensors $\mathcal{X}(t) \in \mathbb{R}^{N\times N\times S}$ at each time point t as shown in Fig.1A. In the next section, we explain the framework for summarizing subject information at the group level for every time point leading to three-mode spatio-temporal tensor that help with tracking of dynamic brain network communities of ASD and TDC.

3.2. Subject Summarization

We concatenate all subjects' BICM computed at a particular time instant resulting in T number of tensors, each with dimension $N \times N \times S$ as shown in Fig.1A. Please note that N denotes the number of ROIs, S denotes the total number of subjects, and T denotes the number of time points. This tensor at one time instant t is denoted as $\mathcal{X}(t)$. Functional connectivity adjacency matrices of a group of subjects are often averaged across all subjects (i.e., group-level FC matrix) [32, 33, 34], to generate a single $N \times N$ matrix. However, averaging across all subjects might lead to loss in inter-subject variability. Thus, to account for this variability, we decompose the 3-mode tensor $\mathcal{X}(t)$ at time instant t using Tucker decomposition (a.k.a. Higher Order Singular Value Decomposition (HOSVD), a generalization of Singular Value Decomposition (SVD) to tensors) [35, 36] as follows:

$$\mathcal{X}(t) = \mathcal{C} \times_1 \mathbf{U}^{(1)} \times_2 \mathbf{U}^{(2)} \times_3 \mathbf{U}^{(3)}, \quad (4)$$

where $\mathcal{C} \in \mathbb{R}^{N\times N\times S}$ is the core tensor and, $\mathbf{U}^{(1)} \in \mathbb{R}^{N\times N}$, $\mathbf{U}^{(2)} \in \mathbb{R}^{N\times N}$, and $\mathbf{U}^{(3)} \in \mathbb{R}^{S\times S}$ are the three orthonormal mode matrices containing left singular vectors corresponding to each of the three modes (Fig.1A). Note that the first two mode matrices $\mathbf{U}^{(1)}$ and $\mathbf{U}^{(2)}$ are equal in case of symmetric adjacency connectivity matrix.

The mode matrices are computed by performing SVD of tensor $\mathcal{X}(t)$, unfolded along corresponding desired mode [35]. For example, the third mode matrix $\mathbf{U}^{(3)}$ contains the left singular vectors of $\mathbf{X}_3(t) \in \mathbb{R}^{S\times N^2}$. Here, we are interested in column space of $\mathbf{U}^{(3)}$ as they span weights of subject summarized connectivity matrix. The first left singular vector ($\mathbf{u}_{3,1} = \mathbf{U}^{(3)}(:, 1) \in \mathbb{R}^{S\times 1}$) of matrix $\mathbf{U}^{(3)}$ captures the most significant functional connectivity energy across subjects [37, 38, 39]. Hence, we utilize $\mathbf{u}_{3,1}$ to obtain the most relevant adjacency matrix of dimension $\mathbf{D}(t) \in \mathbb{R}^{N\times N}$, summarized over all subjects at time instant t. Thus, the subject summarized $\mathbf{D}(t)$ matrix is computed as:

$$\mathbf{D}(t) = \frac{\sum_{s=1}^{S} \mathbf{u}_{3,1}(s)\mathbf{C}^b_s(t)}{\sum_{s=1}^{S} \mathbf{u}_{3,1}(s)}. \quad (5)$$

Similarly, we do subject summarization at each time point. Similar processing across all T time points results in a three-mode spatio-temporal tensor $\mathcal{T}$ of dimension $N \times N \times T$ (Fig.1B), summarized over all subjects as mentioned above. Mode one and two of this tensor correspond to dynamic network connection weights and mode three contains temporal information of the underlying networks.

3.3. Learning Temporal Models using Subject-Summarized Spatio-Temporal Tensor

In this section, we utilize spatio-temporal tensor $\mathcal{T} \in \mathbb{R}^{N\times N\times T}$, obtained after subject summarization as mentioned in the previous section, to learn multiple temporal models for uncovering the underlying DBN communities structure (Fig.1B). To this end, we utilize tensor factorization technique

to represent tensor as a linear combination of multiple rank-one tensors. This can be achieved using parallel factor (PARAFAC) decomposition (a.k.a. canonical decomposition) [40, 36]. The PARAFAC decomposition model for the input three mode tensor $\mathcal{T}$ is written as:

$$\mathcal{T} \approx \sum_{q=1}^{Q} \lambda_q \boldsymbol{a}_q \circ \mathbf{b}_q \circ \mathbf{t}_q, \tag{6}$$

where '$\circ$' denotes the outer product and, $\boldsymbol{a}_q \in \mathbb{R}^{N\times 1}$ and $\mathbf{b}_q \in \mathbb{R}^{N\times 1}$ are the loading vectors corresponding to regions N. Vector $\mathbf{t}_q \in \mathbb{R}^{T\times 1}$ is the time loading vector containing temporal information for tracking the time-varying dynamic profile of communities. Q denotes the number of rank-one tensors (pronounced as number of components hereafter, for simplicity) and λ_q is the singular value corresponding to component q. The decomposition in (6) can also be expressed as:

$$\mathcal{T} \approx \mathbf{D}\mathbf{A}_Q \times_1 \mathbf{B}_Q \times_2 \mathbf{T}_Q, \tag{7}$$

where $\mathbf{D} = diag(\lambda_1, \lambda_2, ...\lambda_Q)$ and $\mathbf{A}_Q = [\boldsymbol{a}_1, ..., \boldsymbol{a}_Q]$, $\mathbf{B}_Q = [\mathbf{b}_1, ..., \mathbf{b}_Q]$, and $\mathbf{T}_Q = [\mathbf{t}_1, ..., \mathbf{t}_Q]$ are the component matrices that contain loading vectors of each of the three modes. $\mathbf{A}_Q$ (or $\mathbf{B}_Q$) in (7) represents ROIs specific loading vectors with their corresponding temporal evolution information is available in matrix $\mathbf{T}_Q$. This is to note that the column dimension of each of the component matrix is Q in the PARAFAC model.

To summarize, given a three-mode tensor $\mathcal{T}$ and the number of components Q, PARAFAC decomposes input tensor into Q number of components. Each component consists of three vectors named as "loading vectors". First two loading vectors are related to regions and the third loading vector contains temporal information for tracking the time-varying dynamic profile of communities.

This is to note that due to symmetric adjacency matrix of size $N \times N$ in the first two modes, component matrix $\mathbf{A}_Q$ is equal to $\mathbf{B}_Q$. Moreover, since modes one and two of tensor $\mathcal{T}$ correspond to adjacency matrices with non-negative values, we add non-negative constraint on both $\mathbf{A}_Q$ and $\mathbf{B}_Q$, and also on the third temporal mode $\mathbf{T}_Q$ in (7). In particular, with non-negative constraint on PARAFAC, we focus on non-negative tensor factorization (NNTF) [41, 42]. Implementation of PARAFAC decomposition was based on the non-negative alternate least squares method [43] combined with a block-coordinate-descent technique [41], also used recently for fMRI experiments [23].

Note that the value of Q in (6) or (7) needs to be defined for PARAFAC decomposition. There are many methods of deciding this value including elbow rule [44], modularity gain [45], core consistency diagnostic [46], or other methods proposed in [47]. We have used the core consistency method to decide the value of Q as has been utilized recently for the case of social networks [48].

Next, we compute Q number of temporal models representing brain regions evolving over time. To this end, we build a temporal model from every q^{th} component using loading vectors contained in component matrices $\mathbf{A}_Q$ (or $\mathbf{B}_Q$) and $\mathbf{T}_Q$. The temporal model of any component q is computed as $\mathbf{V}_1 = \mathbf{A}_Q(:, q) * \mathbf{T}_Q(:, q)' \in \mathbb{R}^{N\times T}$, where $(.)'$ denotes transpose of a vector. Similar computation across all components results in Q number of temporal models $\mathbf{V}_q$ $(q = 1, 2, ..., Q)$ as shown in (Fig.1C). In the next section, we describe our STC framework applied on extracted temporal models to capture and characterize various dynamic brain network communities.

3.4. Spatio-Temporal Clustering (STC) Framework

Clustering of temporal model $\mathbf{V}_q$ along the time dimension (for all Q number of components separately) would capture dynamic brain network communities. To this end, clusters are estimated from every temporal model $\mathbf{V}_q$, $q = 1, 2, ..., Q$ using K-means clustering (Fig.1D) [49]. We chose K-means clustering algorithm for two reasons. First, this problem does not require advanced algorithms beyond K-means and second, K-means is a fast, easy, and simple clustering algorithm.

A parameter search for the best number of clusters K in K-means clustering is done using the silhouette criterion index [50]. The value of K that leads to the highest silhouette value is chosen. Silhouette index value is ranged between -1 to 1 with large positive value indicating good clustering. Note that an initial range of K is set between 1 to 10 as the maximum number of brain networks, generally available in AAL atlas, is eight such as Visual Network (VN), Auditory Network (AN), Bilateral Limbic Network (BLN), Default Mode Network (DMN), Somato-Motor Network (SMN), Subcortical Network (SN), Memory Network (MN), and Cognitive Control Network (CCN) (Table-S1).

We used the Euclidean distance metric for K-means clustering and repeated K-means algorithm 500 times with random initialization of cluster centers. Clustering result that yielded tightest clusters in terms of Euclidean distance metric was considered for further analysis.

3.5. Ranking of Clusters to Obtain Dynamic Brain Network Communities

Once K_q clusters are obtained from each qth component, we require to identify relevant DBN communities from a pool of $C_q^{k_q}$ ($q = 1, ..., Q$ and $k_q = 1, ..., K_q$) clusters. Please note that the term *cluster* refers to results obtained after STC and the term *DBN communities* specifies ranked clusters that imply relevant clusters and hence, denote network communities.

To find relevant DBN communities from all available clusters, we create a novel ranking method. Our ranking method is based on two scores: first is the "connectivity strength" and second is the "temporal strength". Both these scores are defined below. We combine these two scores and define "Combined Cluster Score" in the next subsection that eventually helps with ranking of clusters.

3.5.1. Connectivity Strength

Connectivity strength of a cluster is related to the strength of connectivity between ROIs belonging to the cluster. A relevant and significant cluster will have a group of tightly interconnected ROIs resulting in a high value of connectivity strength. Owing to this, connectivity strength is considered as an important attribute of cluster score.

To this end, first, we compute the connectivity matrix $\mathbf{M}_q$ using the loading vector $\boldsymbol{a}_q \in \mathbb{R}^{N\times 1}$ defined in (6) as $\mathbf{M}_q = \boldsymbol{a}_q \boldsymbol{a}_q' \in \mathbb{R}^{N\times N}$. Since we are only interested in ROIs that are part of the given cluster k_q, we compute desired connectivity matrix as $\mathbf{M}_q^{k_q} = \boldsymbol{a}_{q,k_q}(p)\boldsymbol{a}_{q,k_q}(p)' \in \mathbb{R}^{p\times p}$, where p denotes ROIs that are part of cluster k_q and the corresponding $\boldsymbol{a}_{q,k_q}$ is defined as the *effective loading vector* of regions lying in that cluster.

Each entry $\mathbf{M}_q^{k_q}(i,j)$ informs about the strength of connection between two ROIs i and j. We propose to utilize the sum of all entries in this matrix to compute the connectivity strength of cluster k_q and define this as:

$$\eta_q^{k_q} = \frac{\sum_{i=1}^{p}\sum_{j=1}^{p}\mathbf{M}_q^{k_q}(i,j)}{p^2}, \tag{8}$$

where $q = 1, ..., Q$, $k_q = 1, ..., K_q$, and division by the total number of entries (a measure of number of regions) is a normalization step with respect to the size of the cluster.

3.5.2. Temporal Strength

In this section, we describe the second score (i.e., the temporal strength) required by us to define the proposed cluster score. In general, brain networks are known to be varying over time. Hence, the strength of DBN communities should depend on their temporally varying profile. Thus, the scoring of cluster not only requires the score related to the connectivity strength (see (8)), but also requires a score related to the temporal strength.

To assess the temporal strength of clusters belonging to the qth component, we utilize the time loading vector $\mathbf{t}_q$ of the qth component (as defined in (6)) and define the temporal strength score of all of its clusters as:

$$\tau_q = \sum_{i=1}^{T}\mathbf{t}_q(i), \tag{9}$$

where $q = 1, ..., Q$ and τ_q is the summation of all weight values of $\mathbf{t}_q$ loading vector. Please note that the temporal strength score τ_q is defined commonly for all the clusters computed from the qth component.

3.5.3. Combined Cluster Score

We use the connectivity strength $\eta_q^{k_q}$ defined in (8) and the temporal strength score τ_q defined in (9) to propose the *Combined Cluster Score* (CCS) of each cluster as:

$$CCS_q^{k_q} = \lambda_q \times \eta_q^{k_q} \times \tau_q, \tag{10}$$

where $q = 1, ..., Q$, $k_q = 1, ..., K_q$, and λ_q is the PARAFAC decomposition factor of component q specified in (6). This is to note that CCS defined above is general and is valid for both the overlapping and non-overlapping communities, although our communities are overlapping.

After computing CCS for each cluster using (10), we generate a ranked list of clusters in the decreasing sorted order of CCS. Clusters at the top of the list are considered to be significant and provide useful information about brain network states. These clusters are named as DBN communities. Note that insignificant clusters with low CCS can be filtered

out using thresholding on CCS. However, for simplicity, we consider the top 50% CCS-valued clusters as the desired DBN communities.

4. Experiments and Evaluations

In this section, we elucidate DBN communities in healthy and autism subjects. We computed the phase synchrony based BICM using (3) from a cohort of 26 TDC and 35 ASD subjects obtained from the ABIDE project (see Data Acquisition section).

Subject-level ICM and BICM computed at four random time points of one randomly chosen subject from both TDC and ASD groups are shown in Fig.2. It is difficult to understand the differences across the two groups by visualizing these matrices, representing regional modular connectivity.

After identifying the connectivity matrices at each time instant for all subjects, we computed BICM across all subjects in both the TDC and ASD groups separately and estimated two subject-summarized three-mode spatio-temporal tensors $\mathcal{T} \in \mathbb{R}^{N \times N \times T}$ (refer to section 3.2). The resulting subject-summarized adjacency matrices at three randomly chosen time points are shown in Fig.3 for both the groups. From this figure, we observe that subject-summarized adjacency matrices are weighted compared to the uniform weighting in BICM.

4.1. High Resolution Temporal Model

In the following section, we apply PARAFAC decomposition on three-mode spatio-temporal tensors $\mathcal{T}$ of both the groups (TDC and ASD) and obtain Q temporal models, as discussed in section 3.3. The value of Q is decided according to the core consistency [48]. We approximate the tensor as a sum of Q components as mentioned in (4), where the initial value of Q ranges from 7 to 15. For each value of Q, we computed the core consistency value and the plot of these values as a function of Q is shown in Fig.4. From this figure, we observe that an abrupt change in slope is visible at Q=10. Also, this is to note that a core consistency value above 0.5 is considered acceptable [48] and the corresponding range of Q is considered to be the optimum range.

After estimating the value of Q, we factorized tensor $\mathcal{T}$ into Q components. A typical randomly chosen regional loading vector $\boldsymbol{a}_q$ is shown in Fig.5A and its temporal profile $\boldsymbol{t}_q$ is displayed in Fig.5B for both the TDC and ASD groups. The bottom panel

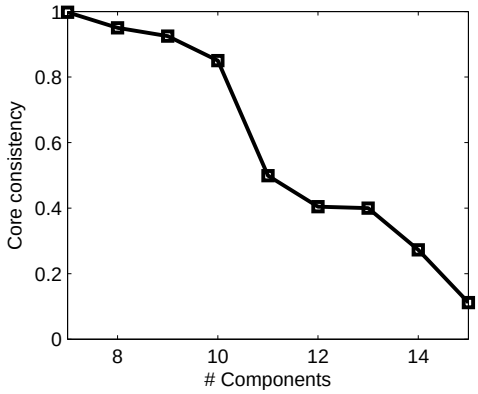

Figure 4: Plot of core consistency with varying number of components.

of Fig.5 shows the corresponding temporal model $\mathbf{V}_q$ depicting inter-regional connectivity strength changing over time. We learned Q temporal models from the PARAFAC components for understanding the evolution of networks over time.

We collected all Q temporal models and applied K-means clustering to identify hub of clusters corresponding to each temporal model. These clusters are ranked by calculating CCS (see section 3.5) to generate most significant dynamic brain network communities as described in the next subsection.

4.2. Community Structure and the Associated Temporal Activity Patterns

Various clusters are identified with K-means clustering on all Q temporal models. Value of K is ranged from 1 to 10 and is decided based on the maximum value of Silhouette index. The pool of clusters are ranked with our CCS in (10), where different ranking of the same region across groups (TDC versus ASD) and clustering with different regions across groups specify differences in activation and connectivity patterns between the two groups.

A typical collection of first 50% clusters (obtained from the pool of total 47 and 54 clusters of the TDC and ASD groups, respectively) based on sorted CCS scores forming dynamic brain network communities are tabulated in Table-2. Tables-3 and 4 illustrate the region-level description of each network listed in Table-2 and lists all the DBN communities in both the groups. We list these communities according to the decreasing order of the CCS score. The temporal evolution of each DBN community in both the groups is presented in Fig.6 and 7, respectively. We observe that the number of communities in ASD is

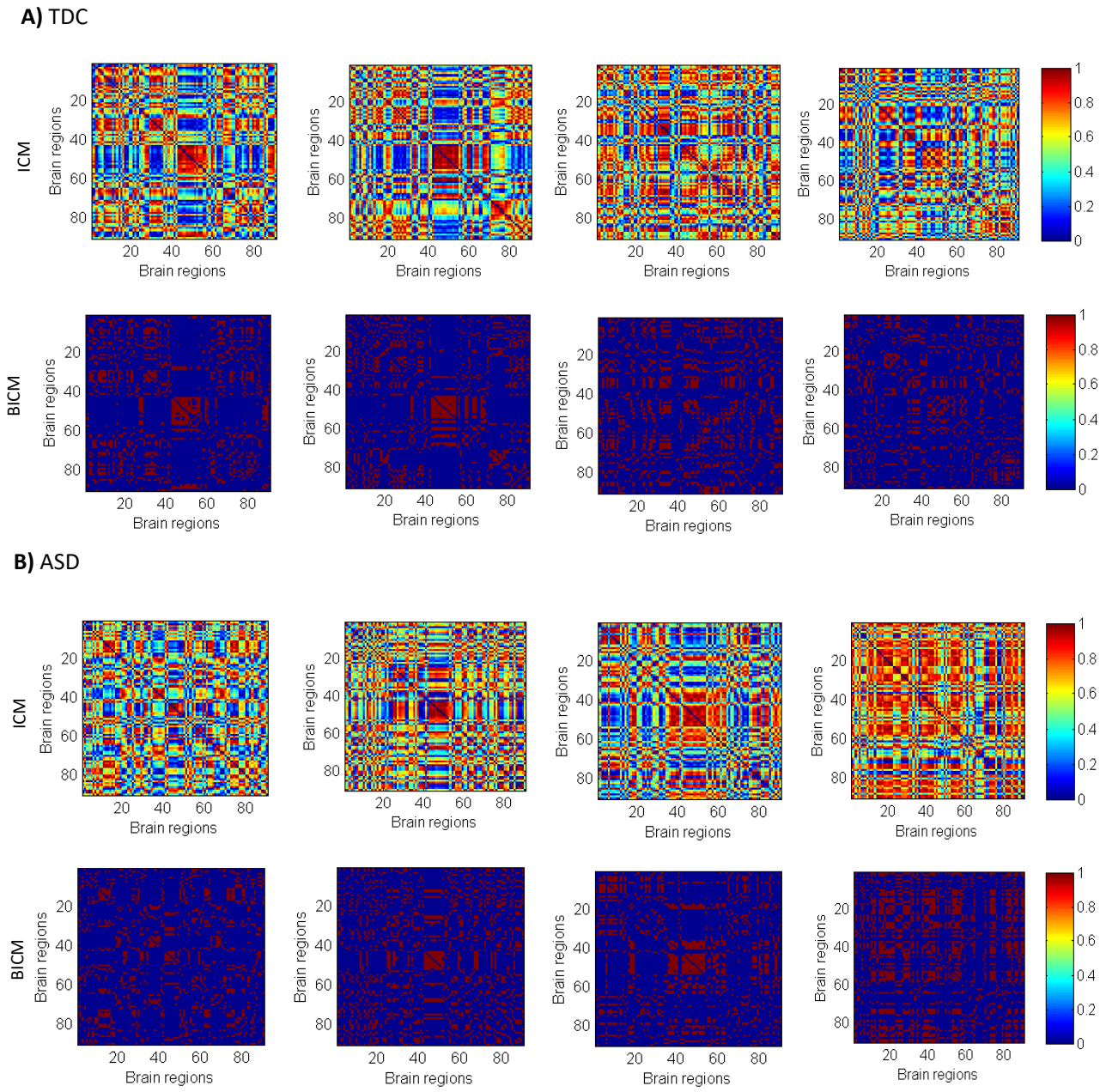

Figure 2: The ICM and BICM at four (randomly chosen) time points (10, 45, 90, and 120) on one subject chosen randomly from both the groups: A) TDC B) ASD.

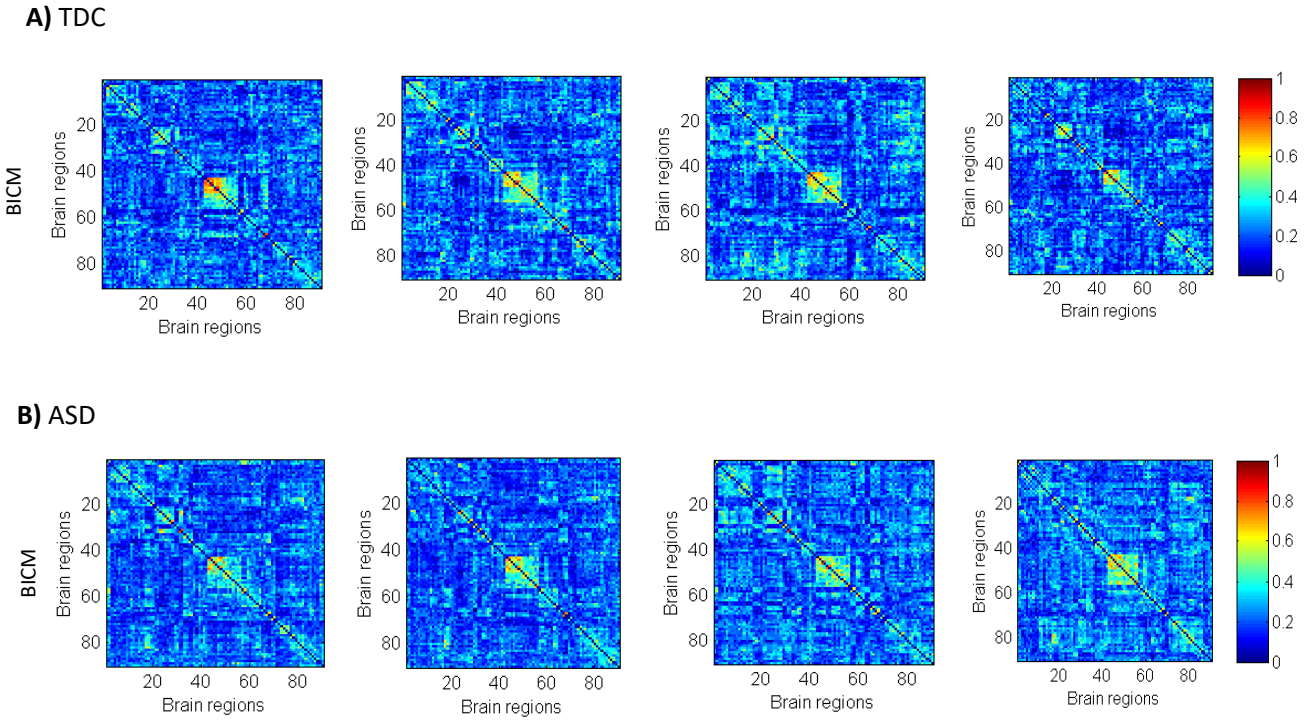

Figure 3: Subject-summarized adjacency matrices at four (randomly chosen) time points (10, 45, 90, and 120) of both the groups: A) TDC B) ASD.

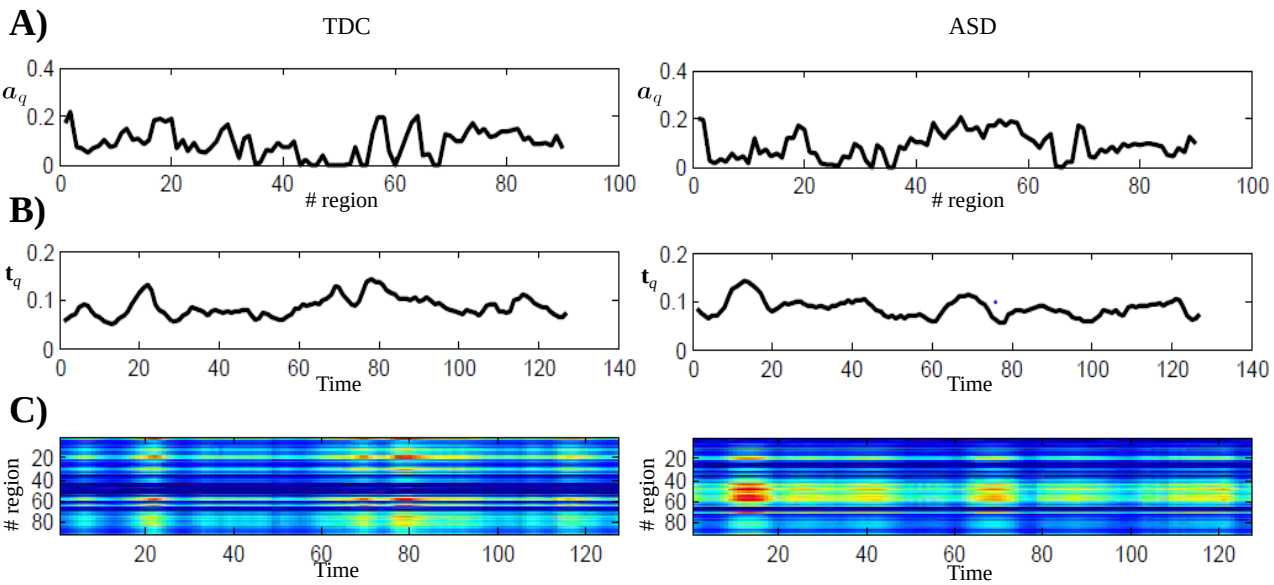

Figure 5: Plot of one randomly chosen regional loading vector $\boldsymbol{a}_q$, its temporal loading vector $\boldsymbol{t}_q$, and the corresponding matrix $\mathbf{V}_q$ for both A) TDC and B) ASD groups.

relatively less compared to TDC. Also, some communities observed in ASD are too small to define or capture the corresponding network structure.

In Table-2, the second and fifth rows report the community size corresponding to each ranked community and their matched brain networks are reported in third and sixth rows. When a community has one or more regions of any of the brain networks including Visual Network (VN), Somatomotor Network (SMN), Auditory Network (AN), Cognitive Control Network (CCN), Default Mode Network (DMN), Bilateral Limbic Network (BLN), Subcortical Network (SCN) and Language Network (LN), the corresponding community is said to be matched with that network. Hence, one community may be composed of multiple brain networks as observed from Table-2.

Our results on TDC group in Table-3 reveal that the first community corresponds to the DMN, BLN, LN and VN, while the second community primarily contains VN. Community 3 consists of nodes of SMN, AN, and SCN. Community 4 containes VN and DMN. Hubs of communities 5 and 6 are involved in CCN, DMN and VN, SMN, respectively. Only one VN region is primarily located in community 7, while community 8 consists of DMN, CCN,and VN. The hub of community 9 is involved in AN, SMN and VN, and so on with the remaining four communities.

Similarly, results on ASD group in Table-4 reveal that the first community is formed with two regions of BLN, while community 2 is primarily involved in the DMN (again connector hub of two regions). Community 3 contains nodes of SMN and VN. Community 4 is involved in BLN and DMN. The hub of community 5 is only involved in BLN, while communities 6 and 7 have regions of SMN, VN and VN, DMN, respectively. Only one VN region is primarily located in community 8, while community 9 is located in SMN, CCN, AN, DMN and LN, and so on for the remaining two communities.

4.2.1. Less Number of Communities with Autism subjects Compared to Healthy Controls

We notice that TDC group results in significant widespread hub of DBN communities with top 50% highest CCS scoring communities (see Table-2 and Table-3). The highest CCS community is comprised of 23 ROIs (community 1 in Table-3) containing the dorsal, orbital, medial and the medial orbital superior frontal gyrus, anterior-posterior cingulate cortex and angular gyrus, forming a network associated with DMN. In general, these regions are strongly active in healthy brain during the rest condition [51]. Similarly, BLN is composed of the olfactory cortex, gyrus rectus and the middle temporal pole regions. Middle and inferior temporal gyrus form the language and visual networks, respectively. On the other hand, ASD group results in only 2 bilateral limbic regions (hippocampus, right parahippocampal gyrus) that are clustered in the first most significant DBN community. Previous studies also reported hyperconnectiviy in the right parahippocampal gyrus of ASD compared to the TDC group [51].

With further decreased value of CCS, TDC group data contains network hubs of VN related regions such as left calcarine fissure (primary visual area), lingual gyrus (primary visual area), the left superior, the left middle and the right inferior occipital gyrus. These regions form part of community 2 in the TDC group. The associated temporally dynamic profile is presented in Fig. 6B. This community is primarily involved with the predominant regions of occipital cortex.

Community 2 of ASD subjects' data exhibits a hub of DMN regions such as medial superior frontal gyrus and the left anterior cingulate cortex. We observe that these regions are also identified in the TDC group (Table-3 community 1a), but are contained in the higher ranked community in the TDC group. In TDC, this community is also denser and contains more regions of DMN. This observation is important because the resting state data is known to exhibit stronger and larger DMN. Further, we note that the anterior-posterior cingulate cortex integration of DMN is lost in the community 2 of ASD group. Such connectivity loss has also been reported in many previous studies [52, 53, 54, 55]. Thus, we note that the DMN network is smaller, less dense, and has connectivity loss in ASD compared to healthy controls.

Next, we compare visual network communities of TDC and ASD groups. Visual network forms part of nine communities in the TDC group, which is expected for a healthy brain in rest condition. Hub of VN communities covers all the regions of primary and high level visual areas, available in AAL atlas, except for the left inferior temporal gyrus region. On the other hand, in ASD group, hub of VN communities is present in only five communities and misses right and left inferior temporal gyrus region. Moreover, communities in ASD have different

Table 2: Identified phase synchrony based overlapping Dynamic Brain Network (DBN) communities

	Community#	1	2	3	4	5	6	7	8	9	10	11	12	13
TDC	Community Size	23	6	12	16	4	4	1	10	5	14	29	5	12
	DBN	DMN-BLN-LN-VN	VN	SMN-AN-SCN-CCN-LN	VN-DMN	CCN-DMN	VN-SMN	VN	DMN-CCN-VN	AN-SMN-VN	CCN-DMN	AN-DMN-BLN-SCN-CCN	VN-DMN-CCN-AN	AN-SCN-CCN-VN-SMN
	Component#	1	3	2	6	7	3	3	4	3	7	5	9	2
ASD	Community Size	3	3	5	5	10	10	9	1	21	6	12	-	-
	DBN	BLN	DMN	SMN-VN	BLN-DMN	BLN	SMN-VN	VN-DMN	VN	SMN-CCN-AN-DMN-LN	DMN-SCN-BLN-LN	DMN-VN-CCN	-	-
	Component#	1	4	2	4	1	2	10	9	3	1	8	-	-

Comparison between TDC and ASD groups with respect to dynamic brain network communities on the basis of their sizes and the brain networks formed for the value of Q=10. Abbreviations: VN- Visual Network; SMN- Somato-motor Network; AN- Auditory Network; CCN- Cognitive Control Network; DMN- Default Mode Network; BLN - Bilateral Limbic Network; SCN - Subcortical Network; LN - Language Network.

rankings compared to the TDC group. For example, primary visual areas such as calcarine fissure, lingual gyrus and cuneus are first present in communities 2 and 4 in the TDC group, while these are part of communities 3, 6, and 7 in the ASD group. Similarly, higher level visual areas extending towards ventral and dorsal visual pathways and superior parietal lobule are present in communities 4 in TDC, while these are part of community 6 in ASD. Thus, we note that VN nodes are part of higher ranked communities (denser and strongly connected) in TDC compared to those observed with the ASD group.

DMN forms part of seven communities in the TDC group, covering all of the DMN related regions. On the other hand, in ASD group, hub of DMN communities is present in six communities with most regions belonging to community 11 compared to community 1 in TDC. In addition, three regions: orbital superior frontal gyrus, Middle frontal gyrus orbital part, and Anterior cingulate right, are missing from DMN communities in the ASD group. These regions are often considered deactivated in ASD. Our findings suggest that these regions are relevant for diagnosis and might act as potential bio-markers in autism disorder. A recent time varying study on ABIDE dataset has noted decreased ranking for precuneus and posterior cingulate gyrus [56]. Similar observation has been made by us. In addition, we also observed reduced ranking in superior frontal gyrus and angular gyrus consonant with global hypoconnectivity noted in these two regions in autism subjects [51].

Seven communities in TDC group reveal full coverage of CCN with all of its regions including bilateral middle frontal gyrus, inferior frontal gyrus, insula and inferior parietal lobule. On the other hand, in the ASD group, hub of CCN is present in only two communities. Also, three regions: middle frontal gyrus, left inferior frontal gyrus (triangular part), and inferior frontal gyrus (orbital part), are missing from CCN in the ASD group. CCN is known to perform attention task and is sometimes also pronounced as dorsal attention network [57, 58]. This network is generally known to be altered in autism disorder as has also been observed by us. This provides further validation to our proposed methodology. We also observed reduced ranking of right insula in ASD (community 9b versus community 3d in TDC) similar to underconnectivity noted in the previous studies [59, 56]. Similar reduced ranking is observed with inferior parietal gyrus region in our study, concordant with underconnectivity finding of [60]. These two re-

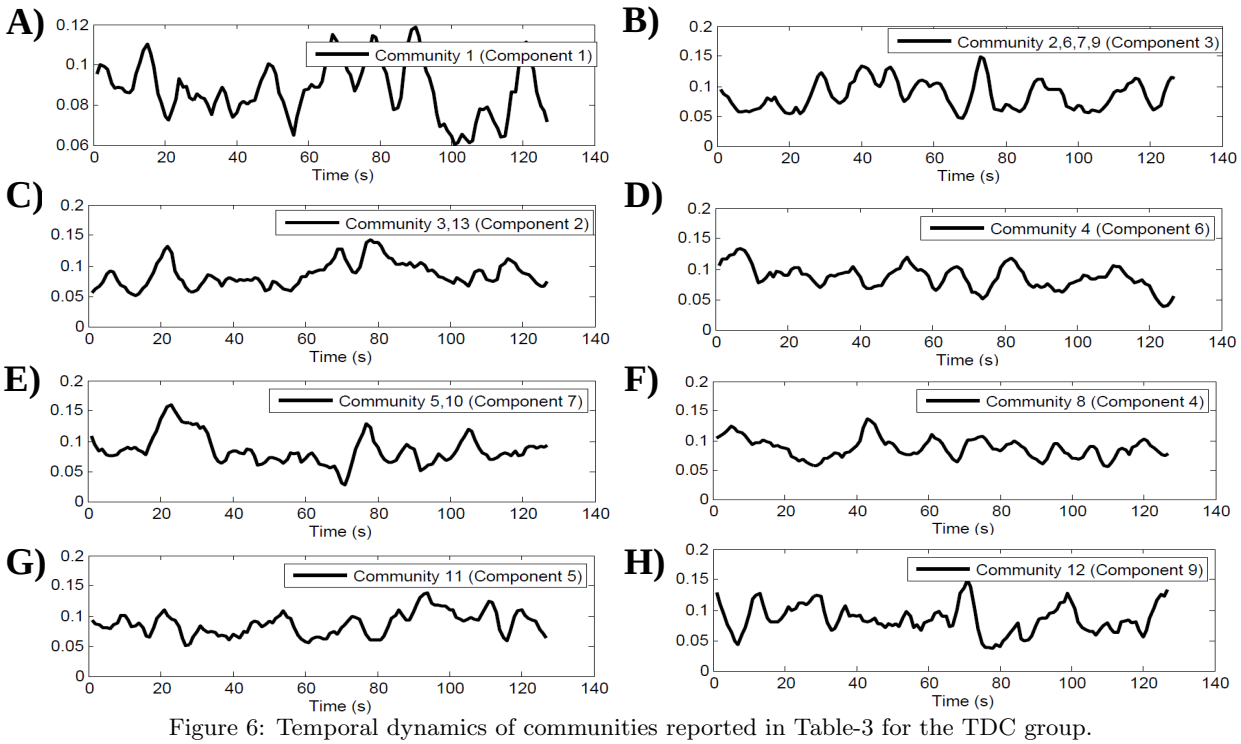

Figure 6: Temporal dynamics of communities reported in Table-3 for the TDC group.

gions together form pareto-insular network responsible for learning and memory [61, 60]. Hypoconnectivity in these regions has already been widely studied in ASD [62, 63] and noted previously in the ABIDE dataset [64, 65].

BLN is observed to be part of two communities (community 1 and 11) in TDC group covering most of the BLN regions that are available in AAL atlas except for left parahippocampal gyrus. On the other hand, in ASD group, BLN regions are observed in four communities with no missing region. The most dense hub of BLN is present in community 5 in the ASD group. Further, we observe that olfactory, gyrus rectus, and temporal pole (middle) regions belong to ranked one community in TDC group compared to community 5 in ASD. However, other bilateral limbic regions such as hippocampus, right parahippocampal gyrus, and amygdala belong to high ranked community in ASD compared to TDC. As aforementioned, previous studies also noted hyperconnectivity in right parahippocampal gyrus for ASD [51].

Somato-motor areas are engaged in four communities in TDC group covering primary motor cortex, primary somatosensory cortex, and supplementary motor areas of SMN available in AAL atlas except for right paracentral lobule. On the other hand, in ASD group, hub of SMN communities are present in three communities, but has missed right supplementary motor area.

Five communities map AN in TDC group covering all of the AN related regions available in AAL atlas. In ASD group, hub of AN communities is present in community 9c including all of the AN related regions. Further, we observe rolandic operculum are included in community 3b in TDC that is higher ranked compared to community 9c as observed in ASD. This suggests hyperactivity in TDC compared to ASD. Such hyperactivity has already been widely noted and has also been reported recently in ABIDE dataset [56].

Language network involving middle temporal gyrus and supramarginal gyrus are present in two communities (1c and 3e) of TDC group. These regions are responsible for language. Similarly, LN is present in two communities (9e and 10d) in the ASD group, although in the relatively lower ranked communities compared to TDC. Differences of connectivity in language networks involving middle temporal gyri has been observed previously. We find that these regions are relevant for diagnosis.

SCN is observed in three communities in TDC group involving putamen, pallidum , caudate nucleus, and thalamus regions. On the other hand, only right putamen region is involved in community 10b in ASD group. It is known that autism children

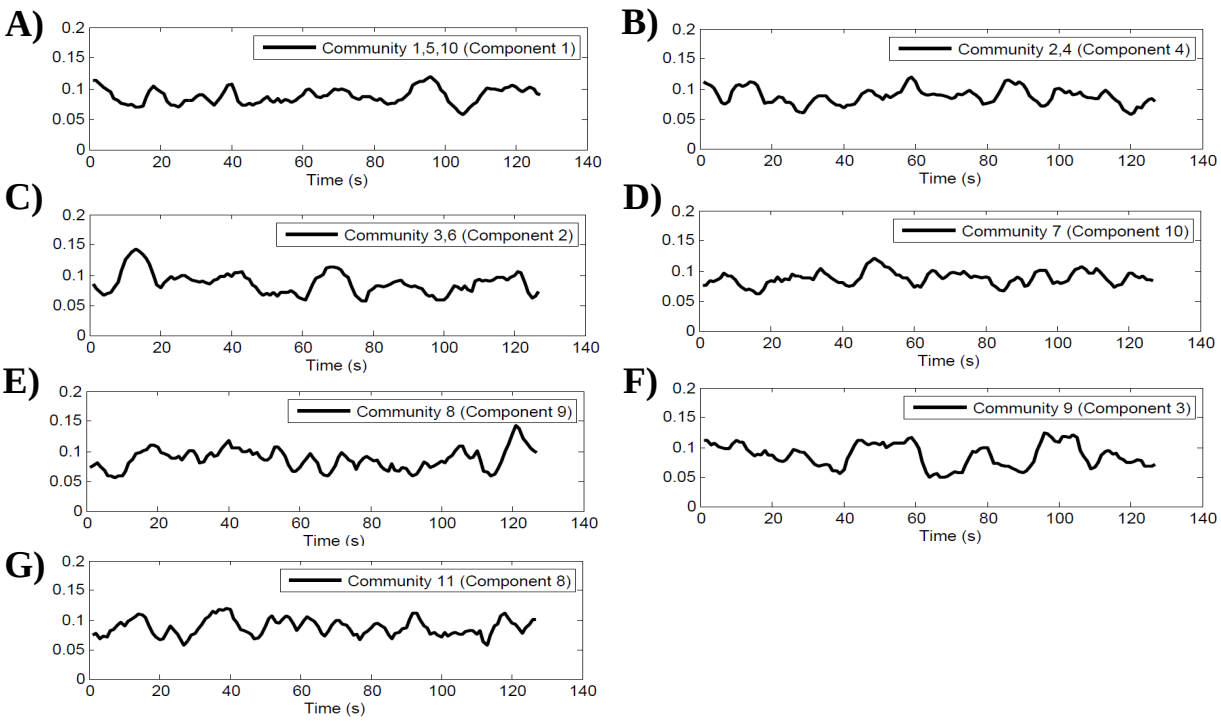

Figure 7: Temporal dynamics of communities reported in Table-4 for the ASD group.

do not show activation in left putamen, pallidum, caudate nucleus, and thalamus regions. It is clearly observed that ASD group exhibits under-activity in SCN and hence, we obtain a fewer number of activated SCN related regions. This indicates that probably there is less activity in the basal-ganglia and thalamus cortex of the brain.

Table 3: List of regions forming communities in the TDC group. Regions are delineated for communities # 1 to 13 (also presented in Table-2).

Community #	DBN	Anatomical Description
1a	DMN	Superior frontal gyrus (dorsolateral)
		Superior frontal gyrus (orbital)
		Superior frontal gyrus (medial)
		Superior frontal gyrus (medial orbital)
		Anterior cingulate cortex
		Posterior cingulate cortex
		Angular gyrus
1b	BLN	Olfactory cortex

Table 3 (continued)

		Gyrus rectus
		Temporal pole (middle)
1c	LN	Middle temporal gyrus
1d	VN	Inferior temporal gyrus right
2	VN	Calcarine fissure left
		Lingual gyrus
		Superior occipital gyrus left
		Middle occipital gyrus left
		Inferior occipital gyrus right
3a	SMN	precentral gyrus
		Supplementary motor area
		Postcentral gyrus
3b	AN	Rolandic operculum
3c	SCN	Putamen right
3d	CCN	Insula right
3e	LN	Supramarginal gyrus
4a	VN	Calcarine fissure
		Cuneus
		Lingual gyrus
		Superior occipital gyrus
		Middle occipital gyrus
		Inferior occipital gyrus
		Fusiform gyrus

Table 3 (continued)

		Superior parietal gyrus left
4b	DMN	Precuneus
5a	CCN	Inferior frontal gyrus, triangular part left
		Inferior frontal gyrus, orbital part left
5b	DMN	Superior frontal gyrus (orbital) left
		Middle frontal gyrus (orbital) left
6a	VN	Calcarine fissure right
		Cuneus
6b	SMN	Precentral gyrus left
7	VN	Fusiform gyrus left
8a	DMN	Middle frontal gyrus, orbital part Right
		Precuneus
8b	CCN	Middle frontal gyrus
		Inferior parietal gyrus
8c	VN	Cuneus left
		Superior occipital gyrus right
		Superior parietal gyrus right
9a	AN	Rolandic operculum
9b	SMN	Supplementary motor area left
		Postcentral gyrus left
9c	VN	Superior occipital gyrus light
10a	CCN	Middle frontal gyrus
		Inferior frontal gyrus, opercular part
		Inferior frontal gyrus,
		triangular part right
		Inferior frontal gyrus,
		orbital part
		Insula right
10b	DMN	Superior frontal gyrus, dorsolateral Left
		Middle frontal gyrus, orbital part right
		Superior frontal gyrus, medial left
		Anterior cingulate cortex
11a	AN	Rolandic operculum
		Heschl gyrus
		Superior temporal gyrus
11b	DMN	Anterior cingulate cortex
		Median cingulate and paracingulate gyri
		Posterior cingulate gyrus
11c	BLN	Hippocampus
		Parahippocampal gyrus right
		Amygdala
		Temporal pole (superior)
11d	SCN	putamen
		pallidum
		Caudate nucleus
		Thalamus
11e	CCN	Insula
12a	VN	Middle occipital gyrus right
		Superior parietal gyrus
12b	DMN	Precuneus right

Table 3 (continued)

12c	CCN	Inferior parietal gyrus left
		Insula
12d	AN	Rolandic operculum
		Heschl gyrus
		Superior temporal gyrus
13a	AN	Heschl gyrus
		Superior temporal gyrus
13b	SCN	Putamen left
		pallidum
13c	CCN	Inferior frontal gyrus, opercular part
		Insula left
13d	VN	Fusiform gyrus right
13e	SMN	Paracentral lobule left

Abbreviations: VN- Visual Network; SMN- Somato-Motor Network; AN- Auditory Network; CCN- Cognitive Control Network; DMN- Default Mode Network; BLN - Bilateral Limbic Network; SCN - Subcortical Network; LN - Language Network. Left and right signify regions in the left and right hemispheres of the brain, respectively.

Table 4: List of regions forming communities in the ASD group. Regions are delineated for communities # 1 to 11 (also presented in Table-2).

Community #	DBN	Antomical description
1	BLN	Hippocampus
		Parahippocampal gyrus right
2	DMN	Superior frontal gyrus (medial)
		Anterior cingulate cortex Left
3a	SMN	Precentral gyrus
		Postcentral gyrus left
3b	VN	Lingual gyrus right
		Fusiform gyrus left
4a	BLN	Gyrus rectus left
4b	DMN	Superior frontal gyrus (Dorsolateral)
		Superior frontal gyrus (medial orbital)
5	BLN	Olfactory cortex
		Gyrus rectus right
		Parahippocampal gyrus left
		Amygdala
		Temporal pole (superior)
		Temporal pole (middle)
6a	SMN	Supplementary motor area left
		Postcentral gyrus right

Table 4 (continued)

		Paracentral lobule
6b	VN	Calcarine fissure left
		Lingual gyrus left
		Middle occipital gyrus left
		Inferior occipital gyrus
		Fusiform gyrus right
7a	VN	Calcarine fissure right
		Cuneus
		Lingual gyrus left
		Superior occipital gyrus
		Middle occipital gyrus
7b	DMN	Precuneus left
8	VN	Calcarine fissure left
9a	SMN	Precental gyrus
		Supplementary motor area left
		Postcentral gyrus
9b	CCN	Inferior frontal gyrus, opercular part
		Inferior frontal gyrus,
		Triangular part right
		Inferior parietal gyrus
		Insula
9c	AN	Rolandic operculum
		Heschl gyrus
		Superior temporal gyrus
9d	DMN	Precuneus left
9e	LN	Supramarginal gyrus
10a	DMN	Superior frontal gyrus, medial orbital
10b	SCN	putamen right
10c	BLN	Gyrus rectus left
10d	LN	Middle temporal gyrus
11a	DMN	Median cingulate and paracingulate gyri
		Posterior cingulate gyrus
		Angular gyrus
		Precuneus
11b	VN	Superior parietal gyrus
11c	CCN	Inferior Parietal Gyrus left

Abbreviations: VN- Visual Network; SMN- Somato-Motor Network; AN- Auditory Network; CCN- Cognitive Control Network; DMN- Default Mode Network; BLN - Bilateral Limbic Network; SCN - Subcortical Network; LN - Language Network. Left and right signify regions in left and right hemispheres of the brain, respectively.

5. Discussion

In this work, we have made an attempt to develop a better understanding of dynamic fluctuations occurring in the resting-state FC of diseased and normal subjects. FC is often computed and interpreted within some fixed time duration. These are known as static brain networks. Recently, results have been reported on the instantaneous interpretation of dynamic FC computed by utilizing the phase difference between pairs of voxels' time series. This phase difference is one of the ways to measure temporal dynamics between regions and is commonly known as phase synchrony.

We examined dynamic reconfiguration of functional brain networks via our proposed method based on ICM, generated from phase synchrony. These matrices are thresholded to preserve the small, but significantly relevant phase synchrony range. Next, subject summarized spatio-temporal tensor is decomposed using NNTF to build multiple temporal models. This is followed by K-means clustering and the ranking of resulting clusters via the proposed CCS measure. This complete process yields appropriate DBN communities. We built DBN communities for both the healthy and autistic subjects to understand the probable alterations of networks in neuro-disorders.

5.1. Hub Structure of dFC States in Healthy Brain

By learning and tracking dynamic brain network communities (Section 2), we find many 'hubs' of commonly reported functional brain networks including the default mode network, visual, cognitive, somato-motor, auditory, bilateral limbic, subcortical, and language networks (Table-3). On analyzing the fMRI data, pre-filtered within 0.01 to 0.08 Hz, we observe considerable activation in the resting state brain of healthy controls. This suggests that binarized instantaneous coupling matrices of phase synchrony contain meaningful information about the large scale brain networks of healthy individuals within 0.01 to 0.08 Hz. Hence, we propose a novel framework of modeling and interpreting dFC that are evolving over time.

We observe that the resting-state DBN communities on TDC, transiently emerge and dissolve in time (Fig. 6), giving rise to dynamic reconfiguration of brain networks. The flexible reconfiguration of brain networks is one of the remarkable characteristics of healthy brain. This allows a healthy subject's brain to suitably adapt to changing environment rapidly and efficiently. Consistent with our findings, temporal fluctuations of dFCs have also been reported earlier using sliding window analysis of fMRI signals on healthy subjects.

In other community detection approaches, regions are usually assigned to only one brain network at one time, while in the real life scenario, a region may be simultaneously performing multiple cognitive and functional tasks and hence, might be a part of multiple overlapping communities at the same time. Because the proposed learning framework of communities involves clustering of various temporal models, extracted from non-negative tensor factorization, it is possible to extract both overlapping and distinct communities. These findings may provide new insights on complex dynamic brain system.

5.2. Within Group Differences in Autism

ASD causes abnormality in functional brain networks via a variety of underlying genetic and acquired causes [56]. Thus, study of brain networks in ASD is a key for understanding the altered functioning in the diseased brain . In order to meet this goal and to have a better understanding of altered brain networks in ASD, we learned the hub structures of DBN communities in the ASD group (Section 2). Compared to DBN networks obtained with TDC (Table 3), we observed relatively less dense hub of DBN communities (Table 4). These findings indicate that network activation differs significantly in ASD from TDC in the resting-state condition.

Our analysis suggests that compared to the TDC group, autism subjects show (1) reduced ranked (and hence, weakly connected) communities of VN, DMN, CCN, BLN, AN, and LN; (2) miss regions commonly found activated as part of VN, DMN, CCN, SMN, and basal-ganglia networks. Furthermore, we observe some bilateral-limbic regions to be belonging to high ranked communities (and hence, are strongly connected), while healthy controls show inverse relationship of ranking of these regions. These findings are consistent with those on altered network measures in the resting state fMRI data of ASD subjects as reported in [52].

Further, we observe missing integration of DMN related regions, anterior and posterior cingulate cortex. This suggests of behavioral problems with deficiency in verbal communication, body language, eye contact, etc. and overall social behavioral deficiency that may lead to decreased ability to conversation [56, 66, 67]. Similarly, reduced ranking and missing activated regions observed on other networks is suggestive of probable alterations in socio-emotional information processing in individuals with ASD.

5.3. Characterizing Regions Distinctive in Autistic Disorder

We carried out detailed investigation on the DBN communities in both the groups. In particular, we want to know regions observed with higher ranking in TDC, i.e., hyper-active regions in ASD and which ones have less ranking in TDC i.e. hypo-active regions in ASD, including missing activated regions in ASD group.

5.3.1. Hypoactive Regions in ASD

Hypo-active regions include the VN regions (calcarine fissure, lingual gyrus, cuneus, fusiform gyrus, superior parietal gyrus, middle and inferior occipital gyrus), DMN regions (precuneus, anterior-posterior cingulate cortex, superior frontal gyrus, angular gyrus, middle frontal gyrus), CCN regions (right insula, inferior frontal gyrus, inferior parietal gyrus), BLN regions (olfactory, gyrus rectus, middle temporal pole), SMN regions (right supplementary motor area, right paracentral lobule), AN regions (rolandic operculum), LN regions (middle temporal gyrus, supramarginal gyrus) and SCN regions (pallidum, putamen, caudate nucleus, thalamus).

5.3.2. Hyperactive Regions in ASD

Enhanced ranking of regions in ASD compared to TDC suggests of hyper-activity of regions in ASD. Hyperactive regions include the BLN regions (left parahippocampal gyrus, hippocampus, amygdala).

5.4. Limitations and Future Directions

The method developed in this work allows us to extract a group level DBN using undirected phase synchroncy measure. However, directionality aspect of brain networks should also be exploited for complete understanding of diseased brain networks. Directed adjacency matrix weights can be estimated using time-shifted version of region time series, as opposed to dFC.

Correlation of Hilbert envelopes also provides information about functional connectivity [68]. However, in this work, we have discarded the magnitude of the analytic signals, i.e. known as Hilbert envelopes. The examination of Hilbert envelops correlations might bring new important findings about brain networks and hence, in future we would like to utilize both envelope and phase information of Hilbert transform for building more robust brain networks.

In Autism, although brain regions show activation on internal or external stimuli, there is altered connectivity between regions and hence, the functional brain networks are affected. This problem leads to reduced attention, difficulty in prioritizing tasks, inhibition in brain required for executing intended tasks, and behavioral problems as stated in the previous section. These problems add difficulty for their caretakers as well. The work carried out in this paper on dynamic functional brain networks can be utilized to develop interventions for these subjects as part of neuro-rehabilitation. We plan to take up this challenge as the future work.

6. Conclusions

In conclusion, a novel methodology has been proposed for estimating dynamic brain network communities that are computed at every time instant. We present application of the proposed framework on ASD subjects demonstrating altered dynamic brain network communities in autism subjects compared to the TDC group. This further supports the hypothesis that autism is a disorder affecting brain networks. We observe that the proposed methodology is able to report changes in large scale networks such as DMN, VN, CCN etc., that is inline with the existing literature. Impaired connectivity in the resting state brain networks is due to the impairment in neuro-psychological function that suggests that study of DBN communities is a potential biomarker in ASD. We have observed reduced as well as enhanced activation in different DBN communities. This suggests that instantaneous functional connectivity can play a key role in the study of reorganization of brain networks.

Acknowledgements

The first author would like to thank Visvesvaraya research fellowship, Department of Electronics and Information Tech., Ministry of Comm. and IT, Govt. of India, for providing the financial support for this work. We also thank ABIDE for sharing the data online.

References

[1] Bullmore, E., Sporns, O., 2009. Complex brain networks: graph theoretical analysis of structural and functional systems. Nat. Rev. Neurosci. 10 (3), 186–198.

[2] Friston, K., 2011. Functional and effective connectivity: A review. Brain Connect. 1 (1), 13–36.

[3] Biswal, B., Zerrin Yetkin, F., Haughton, V. M., Hyde, J. S., 1995. Functional connectivity in the motor cortex of resting human brain using echo-planar MRI. Magn. Reson. Med. 34 (4), 537–541.

[4] Fox, M. D., Raichle, M. E., Sep 2007. Spontaneous fluctuations in brain activity observed with functional Magnetic Resonance Imaging. Nat. Rev. Neurosci. 8 (9), 700–711.

[5] Doucet, G., Naveau, M., Petit, L., Delcroix, N., Zago, L., Crivello, F., Jobard, G., Tzourio-Mazoyer, N., Mazoyer, B., Mellet, E., Joliot, M., 2011. Brain activity at rest: a multiscale hierarchical functional organization. J. Neurophysiol. 105 (6), 2753–2763.

[6] Hacker, C. D., Laumann, T. O., Szrama, N. P., Baldassarre, A., Snyder, A. Z., Leuthardt, E. C., Corbetta, M., 2013. Resting state network estimation in individual subjects. NeuroImage 82, 616–633.

[7] Power, J., Cohen, A., Nelson, S., Wig, G., Barnes, K., Church, J., Vogel, A., Laumann, T., Miezin, F., Schlaggar, B., Petersen, S., 2011. Functional network organization of the human brain. Neuron 72 (4), 665–678.

[8] Thomas Yeo, B. T., Krienen, F. M., Sepulcre, J., Sabuncu, M. R., Lashkari, D., Hollinshead, M., Roffman, J. L., Smoller, J. W., Zöllei, L., Polimeni, J. R., Fischl, B., Liu, H., Buckner, R. L., 2011. The organization of the human cerebral cortex estimated by intrinsic functional connectivity. J. Neurophysiol. 106 (3), 1125–1165.

[9] Chang, C., Glover, G. H., 2010. Time-frequency dynamics of resting-state brain connectivity measured with fMRI. NeuroImage 50 (1), 81–98.

[10] Sakoğlu, Ü., Pearlson, G. D., Kiehl, K. A., Wang, Y. M., Michael, A. M., Calhoun, V. D., 2010. A method for evaluating dynamic functional network connectivity and task-modulation: application to schizophrenia. Magn. Reson. Mater. Phy. 23 (5), 351–366.

[11] Kiviniemi, V., Vire, T., Remes, J., Elseoud, A. A., Starck, T., Tervonen, O., Nikkinen, J., Sep 2011. A sliding time-window ICA reveals spatial variability of the default mode network in time. Brain Connect. 1 (4), 339–347.

[12] Jones, D. T., Vemuri, P., Murphy, M. C., Gunter, J. L., Senjem, M. L., Machulda, M. M., Przybelski, S. A., Gregg, B. E., Kantarci, K., Knopman, D. S., Boeve, B. F., Petersen, R. C., Jack, Jr, C. R., 06 2012. Non-stationarity in the resting brains modular architecture. PLoS One 7 (6), 1–15.

[13] Allen, E. A., Damaraju, E., Plis, S. M., Erhardt, E. B., Eichele, T., Calhoun, V. D., Mar 2014. Tracking whole-brain connectivity dynamics in the resting state. Cereb. Cortex 24 (3), 663–676.

[14] Leonardi, N., Richiardi, J., Gschwind, M., Simioni, S., Annoni, J.-M., Schluep, M., Vuilleumier, P., Ville, D. V. D., 2013. Principal components of functional connectivity: A new approach to study dynamic brain connectivity during rest. NeuroImage 83, 937–950.

[15] Hutchison, R. M., Womelsdorf, T., Gati, J. S., Everling, S., Menon, R. S., 2013. Resting-state networks show dynamic functional connectivity in awake humans and anesthetized macaques. Hum. Brain Mapp. 34 (9), 2154–2177.

[16] Zalesky, A., Fornito, A., Cocchi, L., Gollo, L. L., Breakspear, M., 2014. Time-resolved resting-state brain net-

works. Proc. Natl. Acad. Sci. USA 111 (28), 10341–10346.

[17] Calhoun, V. D., Miller, R., Pearlson, G., Adali, T., 2014. The chronnectome: Time-varying connectivity networks as the next frontier in fMRI data discovery. Neuron 84 (2), 262–274.

[18] Hutchison, R. M., Womelsdorf, T., Allen, E. A., Bandettini, P. A., Calhoun, V. D., Corbetta, M., Penna, S. D., Duyn, J. H., Glover, G. H., Gonzalez-Castillo, J., Handwerker, D. A., Keilholz, S., Kiviniemi, V., Leopold, D. A., de Pasquale, F., Sporns, O., Walter, M., Chang, C., 2013. Dynamic functional connectivity: Promise, issues, and interpretations. NeuroImage 80, 360–378, mapping the Connectome.

[19] Shakil, S., Lee, C.-H., Keilholz, S. D., 2016. Evaluation of sliding window correlation performance for characterizing dynamic functional connectivity and brain states. NeuroImage 133, 111–128.

[20] Hindriks, R., Adhikari, M., Murayama, Y., Ganzetti, M., Mantini, D., Logothetis, N., Deco, G., 2016. Can sliding-window correlations reveal dynamic functional connectivity in resting-state fMRI? NeuroImage 127, 242–256.

[21] Monti, R. P., Lorenz, R., Braga, R. M., Anagnostopoulos, C., Leech, R., Montana, G., 2017. Real-time estimation of dynamic functional connectivity networks. Hum. Brain Mapp. 38 (1), 202–220.

[22] Glerean, E., Salmi, J., Lahnakoski, J. M., Jääskeläinen, I. P., Sams, M., 2012. Functional magnetic resonance imaging phase synchronization as a measure of dynamic functional connectivity. Brain Connect. 2 (2), 91–101.

[23] Ponce-Alvarez, A., Deco, G., Hagmann, P., Romani, G. L., Mantini, D., Corbetta, M., 2015. Resting-state temporal synchronization networks emerge from connectivity topology and heterogeneity. PLoS Comput. Biol. 11 (2), 1–23.

[24] Omidvarnia, A., Pedersen, M., Walz, J. M., Vaughan, D. N., Abbott, D. F., Jackson, G. D., 2016. Dynamic regional phase synchrony (DRePS). Hum. Brain Mapp. 37 (5), 1970–1985.

[25] Demirta, M., Tornador, C., Falcn, C., Lpez-Sol, M., Hernndez-Ribas, R., Pujol, J., Menchn, J. M., Ritter, P., Cardoner, N., Soriano-Mas, C., Deco, G., 2016. Dynamic functional connectivity reveals altered variability in functional connectivity among patients with major depressive disorder. Hum. Brain Mapp. 37 (8), 2918–2930.

[26] Córdova-Palomera, A., Kaufmann, T., Persson, K., Alnæs, D., Doan, N. T., Moberget, T., Lund, M. J., Barca, M. L., Engvig, A., Brækhus, A., et al., 2017. Disrupted global metastability and static and dynamic brain connectivity across individuals in the Alzheimer's disease continuum. Sci. Rep. 7, 40268.

[27] Power, J. D., Mitra, A., Laumann, T. O., Snyder, A. Z., Schlaggar, B. L., Petersen, S. E., 2014. Methods to detect, characterize, and remove motion artifact in resting state fmri. NeuroImage 84, 320 – 341.

[28] Tzourio-Mazoyer, N., Landeau, B., Papathanassiou, D., Crivello, F., Etard, O., Delcroix, N., Mazoyer, B., Joliot, M., 2002. Automated anatomical labeling of activations in SPM using a macroscopic anatomical parcellation of the MNI MRI single-subject brain. NeuroImage 15 (1), 273–289.

[29] Achard, S., Salvador, R., Whitcher, B., Suckling, J., Bullmore, E., 2006. A resilient, low-frequency, small-world human brain functional network with highly connected association cortical hubs. J. Neurosci. 26 (1), 63–72.

[30] Deuker, L., Bullmore, E. T., Smith, M., Christensen, S., Nathan, P. J., Rockstroh, B., Bassett, D. S., 2009. Reproducibility of graph metrics of human brain functional networks. NeuroImage 47 (4), 1460–1468.

[31] Zhang, Z., Telesford, Q. K., Giusti, C., Lim, K. O., Bassett, D. S., 06 2016. Choosing wavelet methods, filters, and lengths for functional brain network construction. PLoS One 11 (6), 1–24.

[32] Thompson, W. H., Fransson, P., 2015. The frequency dimension of fMRI dynamic connectivity: Network connectivity, functional hubs and integration in the resting brain. NeuroImage 121, 227–242.

[33] Robinson, L. F., Atlas, L. Y., Wager, T. D., 2015. Dynamic functional connectivity using state-based dynamic community structure: Method and application to opioid analgesia. NeuroImage 108, 274–291.

[34] Chen, T., Cai, W., Ryali, S., Supekar, K., Menon, V., 06 2016. Distinct global brain dynamics and spatiotemporal organization of the salience network. PLoS Bio. 14 (6), 1–21.

[35] Lathauwer, L. D., Moor, B. D., Vandewalle, J., Mar. 2000. A multilinear singular value decomposition. SIAM J. Matrix Anal. Appl. 21 (4), 1253–1278.

[36] Kolda, T. G., Bader, B. W., Aug. 2009. Tensor decompositions and applications. SIAM Rev. 51 (3), 455–500.

[37] Mahyari, A. G., Zoltowski, D. M., Bernat, E. M., Aviyente, S., Jan 2017. A tensor decomposition-based approach for detecting dynamic network states from eeg. IEEE Trans. Biomed. Eng. 64 (1), 225–237.

[38] Zhang, Q., Wang, Y., Levine, M. D., Yuan, X., Wang, L., 2015. Multisensor video fusion based on higher order singular value decomposition. Information Fusion 24, 54–71.

[39] Thomason, M. G., Gregor, J., 2011. Higher order singular value decomposition of tensors for fusion of registered images. J. Electron. Imaging 20 (1), 013023–013029.

[40] Harshman, R. A., 1970. Foundations of the PARAFAC procedure: Models and conditions for an" explanatory" multi-modal factor analysis. UCLA Working Papers in Phonetics 16 (1), 84.

[41] Kim, J., Park, H., 2012. Fast nonnegative tensor factorization with an active-set-like method. In: High-Performance Scientific Computing. Springer, pp. 311–326.

[42] Cichocki, A., Zdunek, R., Phan, A. H., Amari, S.-I., 2009. Nonnegative Matrix and Tensor Factorizations: Applications to Exploratory Multi-Way Data Analysis and Blind Source Separation. John Wiley & Sons, Ltd.

[43] Paatero, P., Tapper, U., 1994. Positive matrix factorization: A non-negative factor model with optimal utilization of error estimates of data values. Environmetrics 5 (2), 111–126.

[44] Ketchen, D. J., Shook, C. L., 1996. The application of cluster analysis in strategic managment research: an analysis and critique. Strategic Manag. J. 17 (6), 441–458.

[45] Newman, M. E. J., 2006. Modularity and community structure in networks. Proc. Natl. Acad. Sci. USA 103 (23), 8577–8582.

[46] Bro, R., Kiers, H. A. L., 2003. A new efficient method for determining the number of components in parafac

models. J. Chemometrics 17 (5), 274–286.

[47] Chen, Z.-P., Liu, Z., Cao, Y.-Z., Yu, R.-Q., 2001. Efficient way to estimate the optimum number of factors for trilinear decomposition. Analytica Chimica Acta 444 (2), 295–307.

[48] Gauvin, L., Panisson, A., Cattuto, C., 01 2014. Detecting the community structure and activity patterns of temporal networks: A non-negative tensor factorization approach. PLoS One 9 (1), 1–13.

[49] Jain, A. K., Dubes, R. C., 1988. Algorithms for Clustering Data. Prentice-Hall, Inc., Upper Saddle River, NJ, USA.

[50] Rousseeuw, P. J., 1987. Silhouettes: A graphical aid to the interpretation and validation of cluster analysis. J. Comput. Appl. Math. 20, 53– 65.

[51] Monk, C. S., Peltier, S. J., Wiggins, J. L., Weng, S.-J., Carrasco, M., Risi, S., Lord, C., 2009. Abnormalities of intrinsic functional connectivity in autism spectrum disorders,. NeuroImage 47 (2), 764–772.

[52] Hull, J. V., Jacokes, Z. J., Torgerson, C. M., Irimia, A., Van Horn, J. D., 2017. Resting-state functional connectivity in autism spectrum disorders: A review. Front. Psychiatry 7, 205.

[53] Starck, T., Nikkinen, J., Rahko, J., Remes, J., Hurtig, T., Haapsamo, H., Jussila, K., Kuusikko-Gauffin, S., Mattila, M.-L., Jansson-Verkasalo, E., Pauls, D., Ebeling, H., Moilanen, I., Tervonen, O., Kiviniemi, V., 2013. Resting state fMRI reveals a default mode dissociation between retrosplenial and medial prefrontal subnetworks in ASD despite motion scrubbing. Front. Hum. Neurosci. 7, 802.

[54] Cherkassky, V. L., Kana, R. K., Keller, T. A., Just, M. A., 2006. Functional connectivity in a baseline resting-state network in autism. Neuroreport 17 (16), 1687–1690.

[55] Kennedy, D. P., Redcay, E., Courchesne, E., 2006. Failing to deactivate: Resting functional abnormalities in autism. Proc. Natl. Acad. Sci. USA 103 (21), 8275–8280.

[56] Yao, Z., Hu, B., Xie, Y., Zheng, F., Liu, G., Chen, X., Zheng, W., 2016. Resting-state time-varying analysis reveals aberrant variations of functional connectivity in autism. Front. Hum. Neurosci. 10, 463.

[57] Karahanolu, F. I., Caballero-Gaudes, C., Lazeyras, F., Ville, D. V. D., 2013. Total activation: fmri deconvolution through spatio-temporal regularization. NeuroImage 73, 121–134.

[58] Fox, M. D., Corbetta, M., Snyder, A. Z., Vincent, J. L., Raichle, M. E., 2006. Spontaneous neuronal activity distinguishes human dorsal and ventral attention systems. Proc. Natl. Acad. Sci. USA 103 (26), 10046–10051.

[59] Paakki, J.-J., Rahko, J., Long, X., Moilanen, I., Tervonen, O., Nikkinen, J., Starck, T., Remes, J., Hurtig, T., Haapsamo, H., Jussila, K., Kuusikko-Gauffin, S., Mattila, M.-L., Zang, Y., Kiviniemi, V., 2010. Alterations in regional homogeneity of resting-state brain activity in autism spectrum disorders. Brain Res. 1321, 169–179.

[60] Abraham, A., Milham, M. P., Martino, A. D., Craddock, R. C., Samaras, D., Thirion, B., Varoquaux, G., 2017. Deriving reproducible biomarkers from multi-site resting-state data: An autism-based example. NeuroImage 147, 736–745.

[61] Iidaka, T., Matsumoto, A., Nogawa, J., Yamamoto, Y., Sadato, N., 2006. Frontoparietal network involved in successful retrieval from episodic memory. spatial and temporal analyses using fmri and erp. Cereb. Cortex 16 (9), 1349.

[62] Martino, A. D., Kelly, C., Grzadzinski, R., Zuo, X.-N., Mennes, M., Mairena, M. A., Lord, C., Castellanos, F. X., Milham, M. P., 2011. Aberrant striatal functional connectivity in children with autism. Biol. Psychiatry 69 (9), 847–856, genes, Autism, and Associated Phenotypes.

[63] Anderson, J. S., Druzgal, T. J., Froehlich, A., DuBray, M. B., Lange, N., Alexander, A. L., Abildskov, T., Nielsen, J. A., Cariello, A. N., Cooperrider, J. R., Bigler, E. D., Lainhart, J. E., 2011. Decreased interhemispheric functional connectivity in autism. Cerebral Cortex 21 (5), 1134.

[64] Ray, S., Miller, M., Karalunas, S., Robertson, C., Grayson, D. S., Cary, R. P., Hawkey, E., Painter, J. G., Kriz, D., Fombonne, E., Nigg, J. T., Fair, D. A., 2014. Structural and functional connectivity of the human brain in autism spectrum disorders and attention-deficit/hyperactivity disorder: A rich club-organization study. Hum. Brain Mapp. 35 (12), 6032–6048.

[65] Plitt, M., Barnes, K. A., Martin, A., 2015. Functional connectivity classification of autism identifies highly predictive brain features but falls short of biomarker standards. NeuroImage Clin. 7, 359–366.

[66] Assaf, M., Jagannathan, K., Calhoun, V. D., Miller, L., Stevens, M. C., Sahl, R., O'Boyle, J. G., Schultz, R. T., Pearlson, G. D., 2010. Abnormal functional connectivity of default mode sub-networks in autism spectrum disorder patients. NeuroImage 53 (1), 247–256.

[67] von dem Hagen, E. A., Stoyanova, R. S., Baron-Cohen, S., Calder, A. J., 2012. Reduced functional connectivity within and between 'social' resting state networks in autism spectrum conditions. Soc. Cogn. Affect. Neurosci. 8 (6), 694–701.

[68] O'Neill, G. C., Tewarie, P. K., Colclough, G. L., Gascoyne, L. E., Hunt, B. A., Morris, P. G., Woolrich, M. W., Brookes, M. J., 2017. Measurement of dynamic task related functional networks using MEG. NeuroImage 146, 667–678.